FRONT DYNAMICS IN THERMALLY BISTABLE ASTROPHYSICAL FLUIDS*

O. REGEV AND N. SHAVIV

Physics Department, Technion — Israel Institute of Technology, Haifa 32000, Israel

(Received January 17, 1994)

The nonlinear development of thermal bistability in fluids is investigated. One-dimensional models of interacting fronts, treated with the help of singular perturbation theory yield for exponentially (in their size) long time on the way to phase separation. Spatial and temporal perturbation of the cooling may give rise to complex steady patterns. In two dimensions we perform numerical simulations and find for the purely thermal case and for the hydrodynamic case with open boundaries a qualitatively similar behavior — overall growth of the majority domain as a power of the time. Again, stationary complex pattern may be achieved by locking onto spatio-temporal perturbations The hydrodynamic case differs from the purely thermal case in the value of the dynamical exponent (the power with which the correlation length grows in time). The probability of occurrence of critical conditions in an observed astrophysical system is assessed using statistical considerations.

PACS numbers: 95.30. Tg, 05.70. Fh, 05.70. Ln, 68.10. -m

1. Introduction

Inhomogeneities in astrophysical fluids can be sometimes modeled by a two phase medium with dense, cool clouds and hot, tenuous intercloud regions. Optically thin plasmas subject to radiative cooling and heat diffusion, which are thermally unstable and cloudy have been invoked in a number of astrophysical contexts (see *e.g.* Field, Goldsmith & Habing 1969, Karpen *et al.* 1989, Balbus & Soker 1989, McKee & Begelman 1990). These systems are characterized by a heat equation, which for isobaric conditions can be

* Presented at the VI Symposium on Statistical Physics, Zakopane, Poland, September 20–29, 1993.

cast in a reaction-diffusion equation form, resembling the real Ginzburg-Landau equation with a bistable potential functional (*cf.* Elphick, Regev & Spiegel, 1991, hereafter ERS1). However, since the medium is a fluid and the different stable phases have different temperatures (and thus densities), mass advection in addition to heat diffusion is expected and fluid motions have to be included in the model.

The linear analysis of the thermal instability and its properties have been thoroughly studied starting from the work of Field (1965) and the problem has also been approached numerically in various astrophysical contexts (see above references). We shall describe here some recent works on the nonlinear aspects of the instability. In contrast to previous linear and numerical treatments, our attempts have focused on the front and pattern properties combining perturbative, numerical and statistical methods. The key role played by the fronts between the cold and hot gas in such systems has firstly been recognized by Zel'dovich & Pikel'ner (1969). The existence of a stationary front in 1-D for a special value of the pressure was proven, but important questions still remained open. Among them the effects of interactions between fronts, fluid motions, spatio-temporal perturbations, pressure variations and boundary conditions on the dynamics both in 1-D and in the multidimensional case. We shall address these questions in what follows.

2. Formulation of the problem

Neglecting the gravitational, magnetic and other body forces the fluid is described by the basic equations reflecting the laws of mass, momentum and energy conservation (see Field 1965):

$$\frac{\partial \rho}{\partial t} = -\nabla \cdot (\rho \boldsymbol{v}), \tag{2.1}$$

$$\rho \frac{D\boldsymbol{v}}{Dt} = -\nabla p, \tag{2.2}$$

$$\frac{1}{\gamma - 1}\frac{Dp}{Dt} = -\frac{\gamma}{\gamma - 1}\, p\, \nabla \cdot \boldsymbol{v} - \rho \mathcal{L}(p, T) + \nabla \cdot (\kappa \nabla T), \tag{2.3}$$

$$p = \frac{\mathcal{R}}{\mu}\rho T, \tag{2.4}$$

where D/Dt is the Lagrangian derivative. Eq. (2.4) expresses the assumption of a perfect gas equation of state connecting p, the pressure, ρ the density and T the temperature. μ is the mean molecular weight and $\mathcal{R}$ the gas constant. The heat equation (2.3) contains the effects of the "microscopic" processes responsible for the cooling and heating (through the

function $\mathcal{L}$, the net energy losses per unit mass) and heat transport (through the coefficient of thermal conductivity, κ). γ is the adiabatic exponent.

The crucial role of the topology of $\mathcal{L}$ for stability has been established by Field (1965). An S shape of the curve $\mathcal{L}(p,T)=0$ in the $p-T$ plane, for example, will guarantee bistability for certain pressures (see Fig. 1). For a given pressure, such a bistable $\mathcal{L}$ can be expressed with the help of a potential functional having the form of two minima around a maximum (see below). For a special value of p, which we shall call the "critical pressure", p_c, the depth of the minima is equal giving rise to the possibility of existence of two equally stable phases. In 1-D the front between such two phases is stationary and this is the afore mentioned Zel'dovich & Pikel'ner (ZP) front. A single front in 1-D would move only if $p \neq p_c$, because of the asymmetry of the phases. We shall refer to such front motions as "pressure driven". In 2-D, however, the curvature of fronts induces motion even when $p = p_c$. Such "curvature driven" motion towards curve shortening (Rubinstein, Sternberg and Keller 1989) is the primary cause of pattern evolution in this case (see also Gringrod 1991 and ERS1).

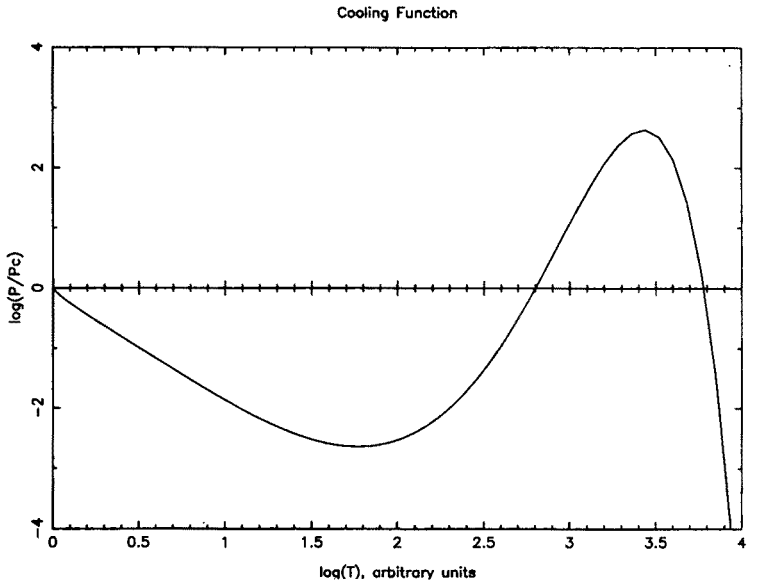

Fig. 1. The bistable cooling curve. Locus of points in the $\log(p/p_c) - \log(T)$ plane for which cooling equals heating. For $p = p_c$ three equilibria, the middle one unstable, exist.

Equations (2.1)–(2.4) can be cast in a non dimensional form if all the physical variables are scaled by their representative values. The natural length unit (the so called "Field length"), l_0, is the typical width of a front

between two thermal phases in the presence of thermal conduction (the effects of heating and cooling balance conductivity). The time unit, the cooling time, is normally much longer than the acoustic time (characteristic time scale of the equation of motion). We shall use henceforth nondimensional equations.

3. Front dynamics in one dimension

In a typical astrophysical application the systems are three dimensional. Therefore the assumption of a 1-D system is not realistic, its only virtue being simplicity. Multidimensional fronts may behave in a radically different way from 1-D fronts (see above and in the next section). Still, the 1-D case may serve as a first step in understanding local properties of fronts, front interaction and other basic physical ingredients of the problem.

ERS1 simplified the problem by neglecting fluid dynamical effects, obtaining essentially a single reaction–diffusion-like equation for the temperature related field $Z(x,t)$ defined as some power of the temperature (related to the constant α arising from the assumption that $\kappa \propto T^{\alpha}$).

$$\frac{\partial Z}{\partial t} = F(Z;p) + Z^{\beta}\nabla^2 Z\,, \tag{3.1}$$

where F is a nondimensional function related to $\mathcal{L}$ and β is a constant expressible as a function of α. In 1-D ∇^2 denotes the second spatial derivative. Since isobaricity was also assumed, p plays the role of a parameter in this equation. For $p \neq p_c$ fast phase separation results, however for p sufficiently close to p_c motion is caused just by front interactions. By using singular perturbation theory ERS1 were able to reduce the problem of $2N$ front (N clouds and intercloud regions) evolution into a system of $2N$ ODEs. In this case phase separation is slow and the timescale of "cloud" lifetimes are exponential in the cloud sizes (large structures could persist essentially indefinitely). It was also demonstrated that the inclusion of a spatial perturbation in the cooling function, which can be undoubtedly expected in an astrophysical system containing also discrete heat sources, may give rise to steady complex patterns. (see Fig. 2).

It is very easy to include fluid flow in 1-D, by using a Lagrangian approach (as was first shown by Meerson 1989). Our next step (Elphick, Regev & Shaviv 1992, henceforth ERS2) was, thus, to use the Lagrangian variable m, defined by $dm = \rho dx$, instead of x, the spatial coordinate in the above problem. The following set of nondimensional equations is obtained:

$$\dot{\rho} = -\rho^2 \frac{\partial v}{\partial m}\,, \tag{3.2}$$

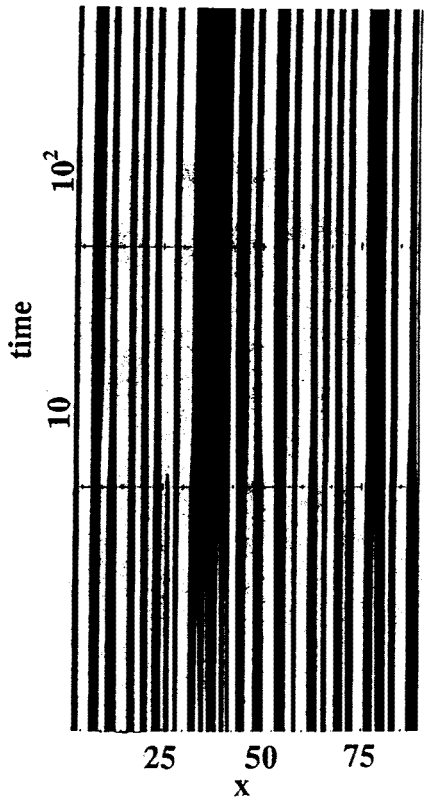

Fig. 2. Time evolution of a fifty front system including a spatial perturbation in the cooling. Steady chaotic pattern persists due to locking (for details see ERS1).

$$\left(\frac{t_s}{t_0}\right)^2 \dot{v} = -\frac{\partial p}{\partial m}, \tag{3.3}$$

$$\dot{T} = \frac{2}{5}\frac{T}{p}\dot{p} - \mathcal{L}(T,p) + \frac{\partial}{\partial m}[\kappa(T)\frac{p}{T}\frac{\partial T}{\partial m}], \tag{3.4}$$

$$p = \rho T. \tag{3.5}$$

In these equations the dependent variables are functions of t and m (an overdot denotes the derivative with respect to t) and γ was set to be 5/3. In equation (3.3) the square of the ratio of the acoustic time, $t_s \equiv l_0/v_{\text{sound}}$, to the cooling time, t_0, appears multiplying $\dot{v}$. The smallness of this ratio justifies the isobaric approximation. The excess (or decrease) in pressure due to the transition of matter from one phase to the other is rather slight and the same pressure prevails in the bulk of both thermal phases.

In this case the problem can again be completely described by a single reduced equation, identical to (3.1), but with m being now the spatial

variable and not x. Thus, all the findings regarding phase separation and possible complex patterns induced by spatial perturbations carry over to this case too (see Fig. 3 and ERS2).

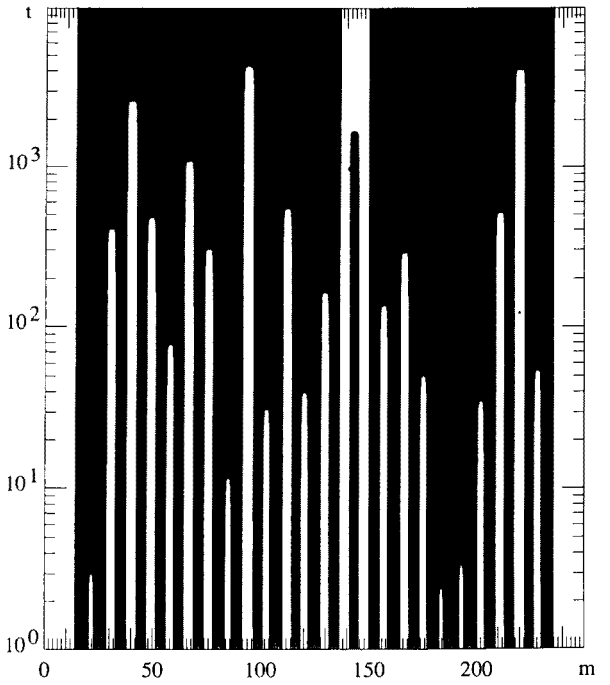

Fig. 3. Same as Fig. 2, but without the perturbation and using the Lagrangian mass variable. Phase separation occurs after a very long time.

Before concluding this section we sketch below the method of deriving front equations of motion in a rather general case (see ERS1 and ERS2 for a detailed derivation).

Consider a cooling function of the generic bistable type (as shown in Fig. 1) denoted, for a given fixed p, by $F(Z;p)$. Let $G(Z,p) \equiv Z^{-\beta}F(Z,p)$ and let $U(Z,p)$ be defined by $G = -\partial U/\partial Z$. Using this "potential", U, the following "free energy" functional can be defined:

$$\mathcal{F}[Z] \equiv \int [\tfrac{1}{2}Z_m^2 + U(Z,p)]dm\,, \tag{3.6}$$

where the integral is taken over the whole system in question. It can be shown (see ERS2) that the *functional derivative* of this functional satisfies:

$$\frac{\delta \mathcal{F}}{\delta Z} = -Z^{-\beta}\frac{\partial Z}{\partial t}\,. \tag{3.7}$$

A steady solution of (3.1) extremizes $\mathcal{F}$. In addition, $\mathcal{F}$ has the property of a *Lyapunov functional* for that reduced PDE. Thus, for $t \to \infty$ one of the steady and stable states will be approached. Consequently, any initial data, which are not a stable steady solution will develop in time in such a way as to increase the extent of the stable phase.

These general considerations remain valid as long as the general shape of U is appropriate (a double "well" potential). Moreover, the behavior of a front solution far from its core and thus near the minima of U (Z_1 and Z_3, say) can be shown to be one of *exponential* approach.

For example, if the cooling function is approximated by

$$F(Z,p) = Z^{\beta}[\Delta^2(Z - Z_2) - (Z - Z_2)^3 - f\log(p/p_c)] \tag{3.8}$$

with f constant and giving, for $p = p_c$ two equally stable states $Z = Z_2 - \Delta \equiv Z_1$ and $Z = Z_2 + \Delta \equiv Z_3$ the front for this case has the form of a hyperbolic tangent (see ERS1,ERS2).

A solution consisting of several fronts is not a superposition of front solutions (the basic equation is nonlinear). For example, a combination of a stationary front followed by its mirror image (ZP antifront) is no longer stationary. It is useful to consider the case in which typical front separations, d, are much larger than their widths ($\sim l_0$). In such a case the solution differs from a suitable superposition of two fronts by only a small amount and we may have recourse to approximation methods.

Let $K(m-m_1)$ be a front (kink) located at m_1 connecting Z_1 at the left to Z_3 at the right and $\overline{K}(m-m_2)$ an antifront (antikink) whose asymptotic behavior is a mirror image of that of K. Up to a small correction the function including both structures can be written as:

$$Z_{K\overline{K}}(m) = \frac{1}{Z_3}K(m - m_1)\,\overline{K}(m - m_2). \tag{3.9}$$

The approximation here is up to order ε, which must be $\sim \exp(-d/l_0)$, since the overlap is only in the exponential tail. This overlap is responsible for the interaction between the fronts and introduces a small correction into their undisturbed (as if there were truly solitary) motion.

The functional $\mathcal{F}$ (3.7) for the function (3.9) differs from the sum of such functionals for K and $\overline{K}$ and the difference reflects the presence of an interaction "energy", defined to be:

$$\mathcal{U}_{int}(m_2 - m_1) = \mathcal{F}[Z_{K\overline{K}}] - (\mathcal{F}[K] + \mathcal{F}[\overline{K}])\,. \tag{3.10}$$

Substitution of (3.9) into (3.10) and the use of the properties of the steady solutions K and $\overline{K}$ gives rise, in lowest order in ε, to the following form of the kink–antikink interaction energy:

$$\mathcal{U}_{\rm int}(m_2 - m_1) = -g\exp[-\gamma_0(m_2 - m_1)]\,, \tag{3.11}$$

where g and γ_0 are positive constants. As the original PDE is first order in time, we obtain for the kink position:

$$\hat{\Gamma}\dot{m}_1 = -\frac{\partial}{\partial m_1}[\mathcal{U}_{\rm int}(m_2 - m_1)] = g\gamma_0 \exp[-\gamma_0(m_2 - m_1)], \qquad (3.12)$$

where $\hat{\Gamma}$ is a constant. The antikink position, m_2, satisfies a similar ODE (for a symmetric U the constants are also the same).

The life-time of an isolated "cloud" (a high density, low temperature and thus low Z region described by an antikink–kink pair) or "intercloud" region can easily be estimated by considering a cloud of size M consisting of fronts at m_1 and m_2, with $M = m_2 - m_1$. If the cloud is isolated it will evaporate as its boundaries (the fronts) attract.

$$\frac{d}{dt}M = -2B \exp(-\gamma_0 M), \qquad (3.13)$$

where $B = g\gamma_0/\hat{\Gamma}$. This implies that an initial cloud of "mass" M_0 evaporates completely in time

$$t_{ev} = \frac{1}{2B\gamma_0}[\exp(\gamma_0 M_0) - 1]. \qquad (3.14)$$

The case of many interacting fronts (with F given by (3.8)), in the nearest neighbor approximation, gives the following equation of motion for the i-th front:

$$\Gamma\frac{dm_i}{dt} = \exp[-\Delta\sqrt{2}(m_{i+1} - m_i)] - \exp[-\Delta\sqrt{2}(m_i - m_{i-1})]. \qquad (3.15)$$

These equations fully describe the system's evolution towards phase separation (Fig. 3) or a stationary pattern pinned onto an external perturbation (if it is included), like the one described in Fig. 2.

4. Two dimensional effects

When one tries to examine the problem in more than one dimension the effect of the interface curvature has to be taken into account. We have already mentioned the fact that even for $p = p_c$ phase separation is expected due to the shrinking of closed domains. Aharonson, Regev and Shaviv (1994) have treated the reduced equation (3.1) numerically in 2-D (in the $x - y$ plane). In order to reduce the full equation set to (3.1) in this case it is necessary, in addition to the isobaric approximation, to neglect fluid motions in the plane. It is possible, in principle, to think of conditions in an

astrophysical systems in which motion is restricted only to the perpendicular direction (by, say, magnetic fields). In any case, as will be shown in the next section, we have found (*a posteriori*) that the results of the full treatment, including advection, produce qualitatively the same type of patterns, the difference manifesting itself mainly in dynamical exponents and effects of boundary conditions.

ARS have concentrated on cases where $p = p_c$ as they are the most interesting. It seems that such conditions should be rather rare, however because of selection effects (see the next section) it is conceivable that these critical conditions prevail in the observed cloud complexes. In addition, Aranson, Meerson and Sasorov (1993) (see also the next section) have shown that even if arbitrary pressure is assumed initially, it relaxes after a short transient to the critical value giving rise to the slow dynamics of front interactions in 1-D, or curvature driven motions in more than 1-D. A system with a *finite* size with velocities vanishing on the boundaries has to be invoked for this purpose, conditions which seem more appropriate for laboratory plasmas than for astrophysical systems (however see below).

The initial conditions for all the numerical calculations consist of a random distribution of Z in the following form: in each square of size 5×5 (out of total 200×200) grid points we set $Z = Z_2 + \delta Z$, where δZ is a random number in the interval $[-0.5, 0.5]$ (Z_2 is the uniform unstable solution).

The parameters chosen in the function $F(Z, p)$ in equation (3.8) are $Z_2 = 2$, $\Delta = 1.9$ with $p = p_c$ (as in ERS1). The runs typically have a duration of about 1000 cooling times.

4.1. Shrinking of a circular domain and merging of two domains

The evolution of a single circular "cloud" of radius R_0 has been found with the help of our code to follow the typical curvature driven front motion (see Rubinstein *et al.* 1989) very well. Since the local velocity of the front is proportional to the curvature, the radius of a circular front evolves according to:

$$\frac{dR}{dt} \propto -\frac{1}{R}, \tag{4.1}$$

with the solution $L(t)^2 \equiv R_0^2 - R^2 \propto t$, where R_0 is the initial radius and L is the typical length scale of the growing domain.

If two circular clouds are initially present, they shrink independently and vanish if they are far apart. However, if they are close enough, their mutual interaction causes them to touch (resembling the form of the figure 8) and merge first before the circularization and shrinking. The interaction of two fronts is exponential in their separation, while the shrinking of each of them is proportional to their curvature. Thus we expect that the critical distance, l_c, between the two circular fronts for merging to occur before

shrinking be such that $\exp[-bl_c] = a/R$, where R is the radius of the smaller circular cloud and a and b are constants. When the distance is less than $l_c = \frac{1}{b}\log(R/a)$, the fronts will merge before shrinking. We have verified numerically that indeed l_c is linear in $\log R$.

4.2. Shrinking of arbitrary domains and the influence of asymmetry of the potential.

It is known, that domain growth kinetics in systems without conservation laws, of the type we have here, follows the rule that the majority domain (the one imposed in our case on the boundary) typical length scale grows like $L \propto \sqrt{t}$ when the potential functional is symmetric (Kandel & Domany, 1990 and references therein). This is plausible when we assume that the solution to (4.1) holds also for arbitrary domain forms.

In the case where $p \neq p_c$ the velocity of the front is proportional to the asymmetry parameter $c_p = p - p_c$ and we have for a circular domain:

$$\frac{dR}{dt} \propto c_p\,, \tag{4.2}$$

with the solution $L(t) \equiv |R_0 - R| \propto t$, thus the typical length scale of the growing domain goes like t in this case.

We have calculated numerically the correlation length, ξ in the system for a variety of random initial conditions of the type described above, and found that after a sufficiently long time $\xi \propto \sqrt{t}$ (for $p = p_c$). Thus, starting with a complicated pattern (like the one depicted in the first panel of Fig.4), the structure develops rapidly (*via* merging and shrinking) and after a few tens cooling times looks like one simply connected blob, with the typical length of the bright domain growing in time as $\sqrt{t}$. The structure develops later *via* curve shortening towards a circular domain and disappear after a long time, with the area of the growing domain changing linearly with time, see Fig. 5 where the fractional area of the shrinking (shaded) domain is depicted as a function of time. It is apparent that the relation becomes linear after a sufficiently long time and it is possible to estimate that the shaded structure will disappear after another $\sim$ 1000 cooling times. In this case we see that an initially complex cloud structure evolves towards a simpler form, persists for a rather long (compared to the cooling time) period and ultimately decays.

As a measure of "complexity" we propose to calculate the fractal dimension of the cloud boundary. Since we are limited by the numerical resolution, the fractal dimension has to be calculated down to some suitable lower cutoff. The method of calculating the fractal dimension is the well known "box-counting method" (see Barnsley 1990). As the lower cutoff we

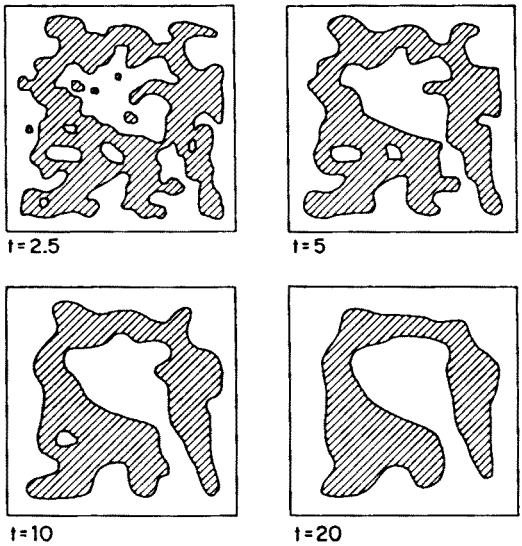

Fig. 4. Short term (up to 20 cooling times) evolution of the system starting from random initial conditions. Cool phase regions are shaded. The four panels are labelled by the time (in cooling times).

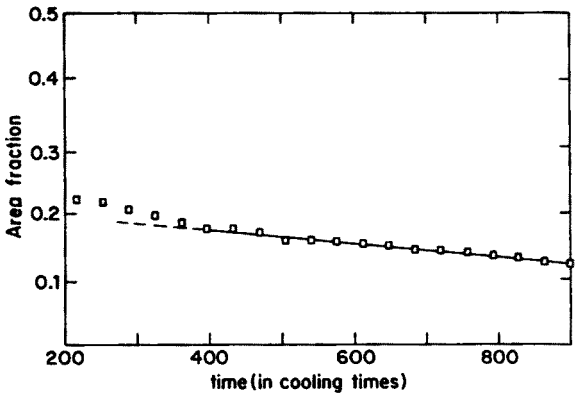

Fig. 5. The area fraction occupied by the dense phase as a function of time for long scale evolution. The clouds area starts to decay linearly with time after a sufficiently long transient.

use a box of 10×10 units and the error bars reflect the changing of this lower cutoff by ± 5 length units. In Fig. 6 the fractal dimension is plotted as a function of time and we clearly see that it becomes practically 1 ("simple" 1-D curve) after a sufficiently long time and stays so.

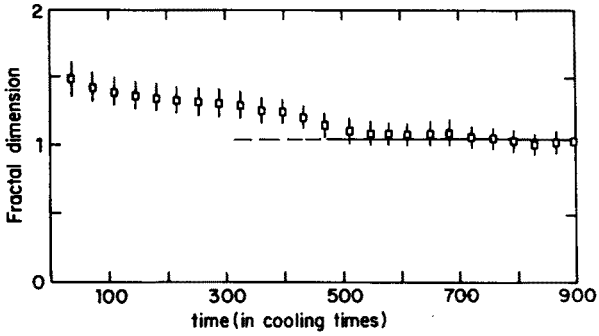

Fig. 6. The fractal dimension of the boundary between the two stable phases as a function of time for the same system as in figure 5. As soon as the cloud boundary smoothens the fractal dimension stays equal to 1.

4.3. Evolution under the influence of spatio-temporal perturbations — complexity.

In a typical astrophysical system the cooling function may include a spatio-temporal variation due to a spatial distribution of the heating sources, which may vary also in time (*e.g.* stars which are born shine and die). Heat sinks may also be present, due to the conversion of heat energy into other forms or increased radiative losses. While these processes may be extremely complicated, we attempt here to model them within our simplistic model as a random perturbation on the averaged cooling function. We thus add to equation (3.1) a term of the form $\delta F(x,y,t) = \varepsilon f(x,y)\sin[(\omega t + \phi(x,y)]$. The domain is divided into 100 squares and in each square $f(x,y) \equiv f_{i,j}$ and $\phi(x,y) \equiv \phi_{i,j}$ $(1 \leq i,j \leq 10)$ are constants. $f_{i,j}$ is a random number between -1 and 1 and the phases, $\phi_{i,j}$ are also random (between 0 and 2π).

The results for the case $\omega = 0.05\omega_0$ ($\omega_0 \equiv 2\pi/t_0$, t_0 is the cooling time) and $\varepsilon = 0.1$) are depicted in Figs 7–9. In Fig. 7 we see that a rather complicated cloud pattern persists for a very long time. It is caused by the persistent spatio-temporal forcing which (not unlike in the 1-D case, see ERS1) gives rise to the "pinning" of the structure by the perturbation. Indeed, in Fig. 8, it can be seen that the area of the shaded region appears to reach a constant value and thus does not continuously decay with time. Moreover, complexity, as reflected by the boundary fractal dimension, is now persistent with the fractal dimension of 1.2 ± 0.1.

Experiments with smaller values of ε gave rise to results which could be regarded as intermediate between no forcing ($\varepsilon = 0$) and this case. The area of the clouds decreased with time, but more slowly that in the unforced case (as $\propto t^q$, with $0 < q < 1$). The fractal dimension continued to decrease towards 1, however its rate of change became extremely slow already for

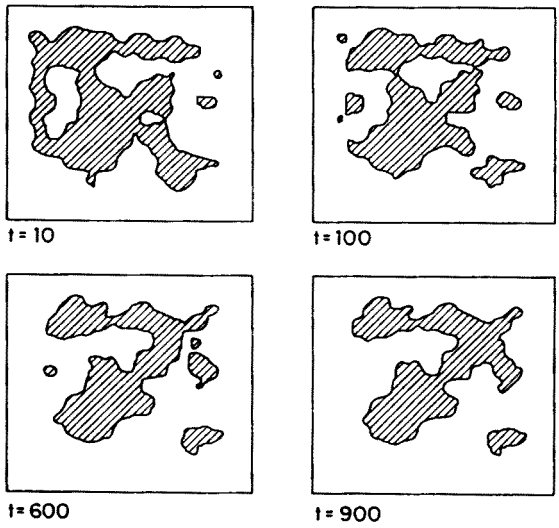

Fig. 7. Same as Fig. 4, but for a long term evolution with a spatio- temporal perturbation on the cooling function of the form described in the text. The perturbation amplitude is 0.1 in this case.

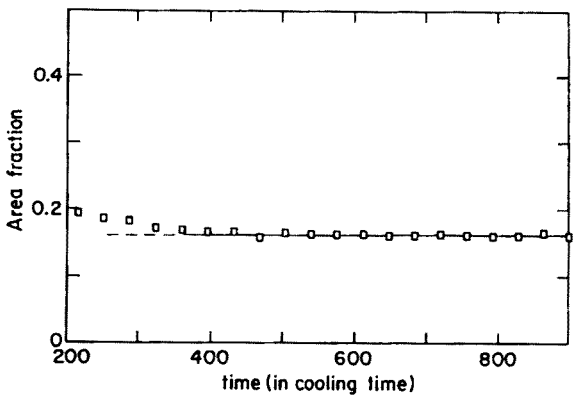

Fig. 8. Same as Fig. 5, but with the perturbation.

$\varepsilon > 0.02$.

For other values of the forcing frequency, ω, we have found that if $\omega \ll \omega_0$, a complex pattern pinned on the spatial perturbation persists even for very small ε. The value of the critical amplitude (ε below which no pattern persists) grows with ω until $\omega \sim \omega_0$. When ω is significantly larger than ω_0 no pinning can be achieved, since the quickly oscillating perturbation averages out to zero over a cooling time.

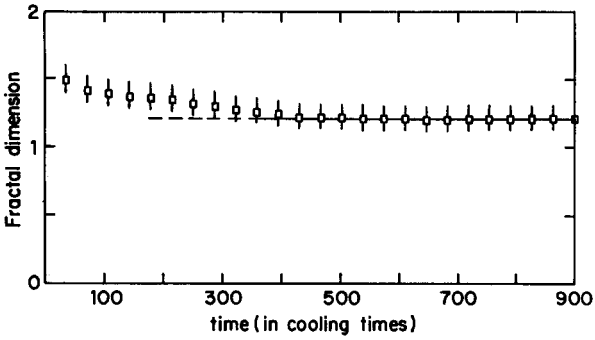

Fig. 9. Same as Fig. 6, but with the perturbation. The fractal dimension levels off at a value ~ 1.2.

5. Effects of advection on multidimensional pattern evolution

When motions are allowed in all directions and we consider a multidimensional problem the full set of equations (2.1)-(2.4) can not be reduced any more to a single equation of type (3.1). The problem may be then approached numerically. Shaviv and Regev (1994) have performed such numerical calculations for various initial and boundary conditions and have found that the results resemble qualitatively the above reported results of the two-dimensional purely thermal-diffusive case. However, the advective motions, necessary for mass conservation, obviously affect several important characteristics of the pattern evolution. Our findings on two such effects are sketched below.

5.1. Dynamical exponents

Equations (2.1)-(2.4) cannot be reduced to a single equation because it is impossible to define a suitable Lagrangian coordinate in the multidimensional case. Still, it is possible to examine a spherically symmetric configuration and define the mass coordinate, m, by $dm = c_0 r^{D-1} dr$ where r is the spatial coordinate, D the dimension and c_0 is a constant related to the density of the inner phase. Assume that the spherical front satisfies an eikonal equation (see Gringrod 1991) of the type

$$N_m + K = c_m \,, \tag{5.1}$$

where $N_m \equiv dm/dt$ is the front velocity in the mass space, K the front's curvature and c_m is proportional to the asymmetry of the phases $(p - p_c)$. In addition, by definition $N_m dt = c_0 r^{D-1} dr$.

We distinguish now between two types of behavior.

(i) When we are near the critical pressure, $p \sim p_c$ and thus $c_m \sim 0$. Using equation (5.1) with $K = (D-1)/r$ for this case we have:

$$c_0 r^{D-1} dr = -\frac{(D-1)}{r} dt . \tag{5.2}$$

Integration yields:

$$r^{D+1} - r_0^{D+1} = -\frac{D^2-1}{c_0} t , \tag{5.3}$$

which means that, as expected, the spherical cloud will shrink because of curvature driven motion. Defining the typical length scale of the growing domain, L, by $L^{D+1} \equiv r_0^{D+1} - r^{D+1}$, we see that $L(t)$ grows with time in this case as:

$$L(t) \propto t^{\frac{1}{D+1}} . \tag{5.4}$$

We get in 2-D: $L(t) \propto t^{1/3}$, and in 3-D:$L(t) \propto t^{1/4}$.

(ii) When p is far from p_c, $c_m \gg K$ and we have $N_m = c_m$. This is the case of a pressure driven motion. Now $c_m dt = c_0 r^{D-1} dr$, yielding:

$$r^D - r_0^D = \frac{c_m D}{c_0} t . \tag{5.5}$$

The cloud will grow or decay according to the sign of c_m and defining again the typical length scale of the growing domain as $L^D \equiv |r^D - r_0^D|$ we get:

$$L(t) \propto t^{\frac{1}{D}} . \tag{2.14}$$

Hence in 2-D: $L(t) \propto t^{1/2}$, and in 3-D: $L(t) \propto t^{1/3}$.

We now make the *assumption* that the power law behavior of $L(t) \propto t^{1/n}$, is the same for both L as defined above (*i.e.* $L^n \equiv |r^n - r_0^n|$ for the system with a spherically symmetric front) and the *correlation length*, ξ, in a general cloudy system viewed as a disordered medium.

Numerical simulations indeed confirm this assumption (up to the accuracy we can measure) as depicted in Fig. 10.

5.2. The occurrence of critical pressure

In the astrophysical context the boundary conditions are notoriously problematic and we have essentially no control of the parameters. It is, thus, relevant to ask what is the probability to have in an observed cloud system

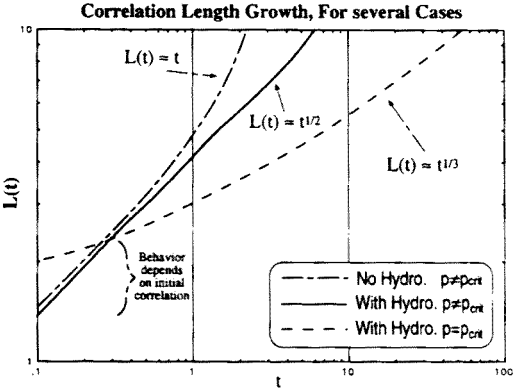

Fig. 10. Numerical result for the correlation length growth in 2-D systems. The correlation length grows as a function of time, giving different asymptotic powers for the relation between L and t.

a certain parameter value, in particular e.g. critical pressure. Consider an ensemble of cloudy systems having a given distribution of initial cloud sizes different ambient pressures. What is the probability as a function of time to observe a system in the critical conditions? This question is particularly relevant to previous works since it was usually assumed that since clouds for which $p = p_c$ live much longer and prevail, systems in which clouds are observed have to be close to the critical conditions.

We first look at a certain system from the ensemble, with a specific pressure. The correlation length behavior, as a function of time, depends on how close is the system to the critical point. As explained before, there are two limits to the behavior of the system's correlation length. Assume that the system is started from some random initial configuration, containing structures on small scales. We expect, thus, that curvature driven motion will be important as long as the small structures are present. Later on, when only large structures are present the role of the pressure in driving the motion becomes dominant.

(i) For small t we are effectively close to $p = p_c$ (i.e. to the critical pressure), and the correlation length goes like $L_1 = a_1\ t^{1/(D+1)}$, where a_1 is a constant.

(ii) For large enough t we are effectively far from $p = p_c$, and we have $L_2 = a_2 y t^{1/D}$ with $y \equiv \pm|p - p_c|^{1/D}$ since c_m is to the first order $c_m \propto (p - p_c)$ and a_2 is a constant. The $+$ sign refers to the case $p > p_c$ while the $-$ is for the opposite case. We have thus effectively two symmetric branches for L as a function of y. The correlation length behavior as a function of time for a fixed y can be seen in Fig. 11.

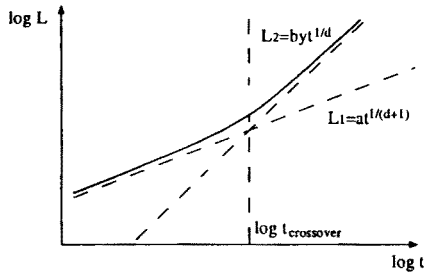

Fig. 11. Correlation length growth in hydrodynamic systems as a function of time. For small t, the correlation length grows while the curvature is dominant, thus $L \propto t^{1/(D+1)}$. For large t the correlation length grows under the influence of the pressure, i.e. $L \propto t^{1/D}$. In between there is a cross over from one behavior to another. This happens at approximately $t = t_{cr}$, depending on the pressure.

Assume now that the correlation length is given by a dimensionless function $f(x)$ of a dimensionless variable x, containing time and y:

$$L = L_0 f(x) . \tag{5.7}$$

The temporal variation will enter only through x (i.e. $x \propto t$) if we assume that scaling exists. Under this assumption:

$$f(x \gg 1) = x^{\frac{1}{D}} \quad \& \quad f(x \ll 1) = x^{\frac{1}{D+1}} , \tag{5.8}$$

$x = 1$ is the crossover point where $L_1 = L_2$. The crossover time is:

$$t_{cr} = \left(\frac{a_1}{a_2 y} \right)^{D^2+D} \tag{5.9}$$

and since $x = 1$ at $t = t_{cr}$ we have:

$$x = \left(\frac{a_2}{a_1} y \right)^{D^2+D} t . \tag{5.10}$$

Thus:

$$L_0 = a_2 \left(\frac{a_1}{a_2} \right)^{D^2+D} y^{1-D-D^2} . \tag{5.11}$$

We next look at an ensemble of systems of clouds placed in different pressures. In Fig. 12 we can see the general behavior of the correlation length as a function of the boundary pressure. In the center there is a region of width

$$\Delta y = 2 \frac{a_1}{a_2} t^{-\frac{1}{D^2+D}} \tag{5.12}$$

corresponding to pressure width

$$\Delta p = 2 \left(\frac{a_1}{a_2}\right)^D t^{-\frac{D}{D^2+D}}, \tag{5.13}$$

where the correlation length behaves as if the pressure is critical for any fixed t.

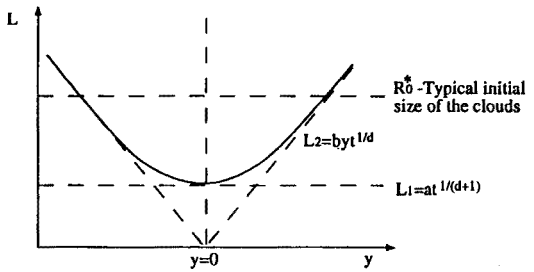

Fig. 12. Correlation length behavior as a function of the deviation of p from its critical value for a given time. For details see text.

Consider now an initial distribution function of cloud sizes for a given ambient pressure given by the function $g(R_0, p)$, defined in such a way that $g\ dR\ dp$ is the number of clouds in a given volume having initial sizes between R_0 and $R_0 + dR$ for a system in which the pressure is between p and $p + dp$. We write:

$$g(R_0, p) = \frac{g_0}{R_0^*} \tilde{g}\left(\frac{R_0}{R_0^*}\right) \tag{5.14}$$

with R_0^* being the typical initial size of a cloud, g_0 a suitable normalization constant and $\tilde{g}$ dimensionless function, whose p independence reflects the fact that we consider the same cloud size distributions for all pressures.

One can now calculate the number of clouds in the central region (where we have curvature influenced behavior). It is equal to the integral over the relevant pressure region (*i.e.* Δp) and over the sizes of clouds that still exist (those with initial sizes greater than the correlation length).

$$N_c = \Delta p \int_{L_1}^{\infty} g(L) dL, \tag{5.15}$$

with $L_1 = a_1 t^{1/(D+1)}$ as given above in *(i)*. This can be rewritten as:

$$N_c = 2\, a_0 \left(\frac{a_1}{a_2}\right)^D t^{-\frac{1}{D+1}}\, h_1(\zeta), \tag{5.16}$$

with $\zeta \equiv L_1/R_0^*$.

Like $\tilde{g}(u)$, $h_1(u)$ is a dimensionless function defined by:

$$h_1(u) \equiv \int_u^\infty \tilde{g}(v)dv \tag{5.17}$$

The number of clouds in the y-region in which there is pressure driven motion is:

$$N_{\rm p} = 2 \int_{\Delta p/2}^{\infty} \int_{L_2}^{\infty} g(L)dLdp, \tag{5.18}$$

where $\Delta p/2 = (a_1/a_2)^D \; t^{-(1/D+1)}$ and $L_2 = a_2 \; y \; t^{1/D}$ as given in *(ii)*. This can be written also as

$$N_{\rm side} = 2g_0 \int_{\Delta p/2}^{\infty} h_1 \left(\frac{L_2}{R_0^*}\right) dp. \tag{5.19}$$

Remembering that $dp = Dy^{D-1}dy$ (for $y > 0$) and defining another dimensionless function:

$$h_2(u) \equiv \int_u^\infty Dv^{D-1}h_1(v)dv \tag{5.20}$$

gives:

$$N_{\rm p} = 2g_0 \left(\frac{R_0^*}{a_2}\right)^D \frac{1}{t} \; h_2(\zeta). \tag{5.21}$$

Therefore the ratio between the number of clouds of the different regions is:

$$\frac{N_{\rm c}}{N_{\rm p}} = \zeta^D \frac{h_1(\zeta)}{h_2(\zeta)}. \tag{5.22}$$

Let us examine this result for two typically expected initial cloud size distributions. If we start with an exponential distribution having a typical radius of R_0^*, for the initial radii of the clouds, the ratio between the number of clouds in the curvature driven zone and in the pressure driven zone would be proportional to ζ. Therefore most clouds will seem to develop according to pressure driven evolution (*i.e.* p effectively different from p_c) until the correlation length in the system will reach the typical initial cloud size (*i.e.*

$\zeta \approx 1$), then the majority of the most clouds will seem to develop then according to curvature driven evolution (*i.e.* p effectively equal to p_c).

In the case of an initial power law distribution, we have

$$g(R_0) \propto \frac{1}{R_0^\gamma} \quad \Rightarrow \quad \frac{N_c}{N_p} = \gamma - (1+D). \tag{5.23}$$

Thus, for a power law initial distribution, there will always be a constant ratio between the number of clouds in the curvature driven zone and the pressure driven zone. It will be less than one (*i.e.* dominated by pressure driven clouds) only if we have $1 + D < \gamma < 2 + D$ since because of obvious constraints, we must always have $\gamma > 1 + D$.

It is, therefore, not obvious that while looking at an ensemble of cloudy systems at different pressures, we will indeed see, as time goes on, more and more clouds in the curvature driven zone, relatively to the number of clouds in the pressure driven zone. Hence, the assumption made previously that the clouds in the pressure driven zone, that live longer, will be seen more frequently by observers, is not necessarily correct. In the case of an initial power law distribution of the clouds, this assumption will be correct only if we have enough small clouds (γ is large enough). When we have an initial distribution of clouds with a typical initial radius, such as an exponential distribution, this assumption will be correct if the correlation length in the curvature drive zone is larger than the typical initial cloud size, which of course happens always for large enough t.

This work was supported in part by the Fund for the Promotion of Research at the Technion and by the Basic Research Foundation of the Israel Academy of Sciences. We thank Prof. Fuliński and Drs. Rościszewski and Zygadło for their warm hospitality at the Zakopane meeting.

REFERENCES

Aharonson, V., Regev, O., Shaviv, N., *Astrophys. J.* (1994) (in press).
Aranson, I., Meerson, B., Sasorov, P.V., *Phys. Rev.* **E47**, 4337 (1993).
Balbus, S.A., Soker, N., *Astrophys.J*, **341**, 611 (1989).
Barnsley, M., *Fractals Everywhere* Academic Press, San Diego 1988.
Elphick, C., Regev, O., Spiegel, E.A., MNRAS **250**, 617 (1992) (ERS1).
Elphick, C., Regev, O., Shaviv, N., *Astrophys. J* **392**, 106 (1992) (ERS2).
Field, G.B., *Astrophys. J* **142**, 531 (1965).
Field, G.B., Goldsmith, D.W., Habing, H.J., *Astrophys. J.* **155**, L149 (1969).
Kandel, D., Domany, E., *J. Stat. Phys.* **58**, 685 (1990).

Karpen, J.T., Antiochos, S.K., Picone, J.M., Dahlburg, R.B., *Astrophys. J.* **338**, 493 (1989).
McKee, C.F., Begelman, M.C., *Astrophys. J.* **358**, 392 (1990).
Meerson, B. *Astrophys. J.* **347**, 1012 (1989).
Rubinstein, J., Sternberg, P., Keller, J.B., SIAM *J. Appl. Math.* **49**, 116 (1989).
Shaviv, N., Regev, O., *Phys. Rev. E* (1994) (submitted).
Zel'dovich, Ya.B., Pikel'ner, S.B., *Sov. Phys.- JETP* **29**, 170 (1969).